Centrifuge modelling of inertial loading and pore pressure effects beneath sand slopes

N.K. Pilgrim

CUED/D-Soils/TR281 (1994)

Centrifuge modelling of inertial loading and pore pressure effects beneath sand slopes

N.K.PILGRIM[1]

The experimental data from an investigation of the response of sand slopes to centrifuge model earthquakes is presented. In each test a condition of steady state seepage was established parallel to the base of the model slope before triggering a single earthquake. Discrete slip planes are not observed, the predominant form of instability beneath both steeper and more gentle slopes is shear strain deformation, which is continuous, though not linear, with depth. The results suggest that inertial loading is predominant in mechanisms associated with the deformation of slopes of moderate inclination, while transient pore pressure increase (and subsequent gravity effects) predominate in mechanisms associated with the deformation of more gentle slopes.

KEYWORDS: gravity, inertial loading, shear strain, slopes, pore pressure.

INTRODUCTION

The proceedings of recent Japanese-U.S. co-operative research now provide a significant source of case history data concerning liquefaction induced ground displacements on gently inclined ground. For example:

'Nicholas Kumoi Pilgrim, M.A., Ph.D. Visiting fellow, Department of Civil Engineering, University of Tokyo.

(a) In the Ohgata area of Niigata City during the 1964 Niigata earthquake (Yasuda et al, 1989). Surface displacements of over 6 m took place towards the Tsusen River above a liquefiable soil layer 4 m thick with an average slope of "only 0.5 %" (percent).

(b) On the west side of the Upper Van Norman Reservoir as a result of the 1971 San Fernando earthquake (O'Rourke et al, 1989). Surface displacements of up to 3.0 m took place above a layer of artificial fill overlying a liquefiable layer of alluvium of maximum thickness 6 m and basal slope of "1 ^{o} to 2" " (degrees).

In the last case "... damage was especially severe for buried conduits", which is the primary concern of the Japanese-U. S. research programme.

Shaking table tests presented by Sasaki et al (1992) and Towhata et al (1992) have clarified a number of the issues raised by these case histories: permanent displacement develops downslope due to gravity; lateral displacement is greatest at the surface of a liquefied layer, while negligible at the base; the unsaturated surface layer moves together with the liquefied sublayer without slip at their interface.

Ground displacement was thus shown to be a result of shear strain in the softened layer below the saturation surface and not due to the formation of discrete slip planes. However, as the authors (Sasaki et al) themselves point out, there is no possibility of using lg shaking table models to investigate moment by moment displacement: in terms of replicating in situ behaviour, the rate of pore pressure dissipation is too fast and the models do not therefore have sufficient time to develop large displacements in

a softened state. The exact nature of continuous deformation, and in particular the relative significance of inertial loading effects and transient pore pressure increase (gravity effects), has remained uncertain.

The importance of centrifuge modelling in research involving excess pore pressures, the build up of strain and the degradation of stiffness and strength has been outlined by Steedman (1989). Two of the most significant errors introduced by modelling at 1 g are made apparent by the roles of interlocking (dilatancy) and confining pressure in Bolton's equations for peak shearing resistance (Bolton, 1986). To quote Steedman:

"One of the primary difficulties in the construction of models at lg is to make allowance for the enhanced tendency for an aggregate of interlocking particles to dilate at low stress levels...

... At very low stress levels grain crushing is usually assumed to be insignificant but even at moderate stress levels crushing of particle asperities contributes to a highly non-linear relationship for stress-strain relationships as a function of confining pressure."

A third feature is:

"... the important role that pore pressure migration during shaking plays in the response of the system."

This last point is the incompatibility noted above by Sasaki et al between time associated with pore pressure dissipation and time associated with motion. Compatibility between these two scaling relationships for time is achieved by reducing the coefficient of permeability, and in dynamic centrifuge modelling one solution is the use of high viscosity silicon oil as the pore fluid (for example Pilgrim, 1994).

In this paper the results from an experimental programme carried out on the Cambridge Geotechnical Centrifuge are presented. The main objective is to establish empirical data with which to clarify the nature of continuous deformation beneath sand slopes of gentle to moderate inclination, and in particular the relative significance of inertial loading effects and transient pore pressure increase (gravity effects).

THE EXPERIMENTAL PROGRAMME

The principles of centrifuge modelling and dynamic tests are discussed by Schofield (1980, 198 1). The mechanical properties of sand within a prototype slope depend on the stress state, which is replicated in a centrifuge model of length scale l/N subject to a radial acceleration field of Ng. If certain scaling relationships are satisfied the response of the model to seepage forces and earthquake loading is the same as that of the prototype. The "Bumpy Road" facility at Cambridge simulates earthquake loading by providing ten cycles of predominantly horizontal acceleration.

Data from two series of tests is presented: Series B tests (NP1 1 to NP14) were of 18" slope and 40 % relative density, and Series C tests (NP 15 to NP 18) were of 6" slope and 40 % relative density. All the centrifuge tests were carried out at 80g, for which

the fundamental frequency of the model earthquake is about 120 Hz. The models were made from Nevada sand, the properties of which are presented in Table 1 together with constant head permeability (Arulmoli et al, 1992).

The experimental package is shown in Figure 1, and Series B and C slopes can be seen in cross-section in Figures 2 and 4. In terms of the Bumpy Road Box co-ordinate Z (Figure 1), the base slope extends from Z = +9 mm to Z = -320 mm in Series B models, and from Z = +20 mm to Z = -350 mm in Series C models. The slopes are of width 300 mm and depth 80 mm (Series B) or 100 mm (Series C).

The supporting structure was made from marine plywood. Stainless steel plates were fitted to reduce side friction and, for transmission of shaking, sand was glued to the base slope. In a number of the tests a stainless steel plate was also fitted over the horizontal base at the toe of the slope. The plywood support was tilted across the width of the slope to account for the earth's gravity during flight, which acts as a small component perpendicular to radial acceleration. The inclination of all planes was adjusted to account for the inflight radial acceleration field and spatial curvature. The effects of variation in acceleration with increasing radius and the coriolis effect are negligible (Pilgrim, 1994).

A 12.40 litre tank was located inside the Bumpy Road Box (itself of dimensions 900 x 480 x 220 mm), and air pressure applied to raise silicon oil from the tank to a reservoir at the top of the slope. The level of oil in the reservoir was monitored by a pore pressure transducer, and the air pressure to the tank adjusted as required. The reservoir

was filled with coarse sand, confined by a steel mesh and a steel grid which was screwed to the plywood base. In order to reduce erosion at the top of the slope the coarse sand was graded into fine Nevada sand at the reservoir/model interface. As a precaution against preferential seepage transducer leads were tied to pins above the model surface and not taped to the side of the plywood support. This method also prevents the leads from restricting movement of the transducers when the slope fails. Series B models NP12 and NP14 and all Series C models were made with a coarse sand drain which extends beneath the toe to control the pattern of seepage and prevent surface erosion.

Each model was made by pouring sand from a suspended hopper. The Bumpy Road Box was first tilted back, and the model slope was poured in three horizontal layers. To pour a model of uniform void ratio both the hopper height and the rate of discharge must be constant. The relative density was calculated from the mass of sand poured and from the volume of sand which was established after measuring the surface profile of the slope. A relative density of about 40 % was obtained by pouring from a height of 10 cm +/- 2 cm with a rate of discharge of 200 cc per minute +/- 10 cc.

Accelerometers (ACC), pore pressure transducers (PPT) and linear variable differential transformers (LVDT) were used. The basic array of transducers is shown for Series B models in Figures 2 and 3, and for models NP15 and NP17 in Figures 4 to 7 (Bumpy Road Box co-ordinates on the longitudinal, Z, axis are marked in mm). Internal deformation and surface movement were found by measuring the position before and after testing of line markers of coloured sand. Lines were placed across the entire

width of the slope, at intervals of 100 mm, on the surface of each layer of sand poured during model construction. In Series B models (of slope depth 80 mm, or 6.4 m in the prototype) the lines were placed on the surface and at depths of 20 mm and 50 mm, and in Series C models (of slope depth 100 mm, or 8.0 m in the prototype) the lines were placed on the surface and at depths of 20 mm and 60 mm. The movement of line markers was found by post-flight dissection of the model.

The models were dry at the start of each centrifuge test. Oil was introduced to the reservoir during flight after 80g was established. The development of seepage was monitored by a line of pore pressure transducers along the slope base. Figures 8 and 9 (which are adjusted to show flow in a vertical gravity field), for Tests NP12 and NP16, show typical records. Steady state seepage was achieved by maintaining a constant oil level in the reservoir, and the earthquake fired.

EXPERIMENTAL DATA AND OBSERVATIONS

Model details are summarised in Table 2, and some time-records of acceleration and pore pressure are presented for Tests NP14, NP15 and NP17 in Figures 10 to 14 (in which prototype acceleration is recorded as a percentage of the earth's gravity, g).

Results: Series B

(a) In Tests NP11 and NP13 a stainless steel plate was fitted over the horizontal base at the toe of the slope, and the models were built without a toe drain. As a result of the earthquake a wedge of sand failed (graben formation) at the toe of the slope and a pressure ridge formed at the front edge of the toe.

(b) In Tests NP12 and NP14 the horizontal base at the toe of the slope was coated with sand, and the models were built with a drain to control seepage from the toe. There was no evidence of graben formation following the earthquake. In Test NP12 an extended pressure ridge formed over the toe of the slope, but in Test NP14 shallow gullies and areas of wash covered an extensive part of the surface and indicate the emergence and flow of oil.

(c) The acceleration peaks recorded in the surface layer (ACC 3441 in Figure 13 for Test NP14) are characterised by truncation and an extended "spike". A phase lag accumulates through the layer, but never exceeds 40" (measured at the end of successive negative peaks). The increase in this phase lag during cycles 5, 6 and 7 possibly correlates with an increase in strain softening due to larger amplitude stress cycles, but in general the negative pore pressures shown in Figure 10 may be associated with a stiffening of the sand mass.

(d) Video film shows that in all the Series B tests downslope movement of the slope surface took place predominantly during the earthquake and not before. At the moment of the earthquake the surface of the sand slope is seen to move away from the steel grid at the reservoir/model interface. There is no visible evidence at the surface (such as scarp formation) to suggest that sand collapsed to fill the gap. In addition, the low permeability of the Nevada sand buffer layer within the reservoir prevents the rapid seepage of silicon oil to fill this gap. As a result, this upslope face is not subject to hydrostatic or hydrodynamic fluid pressure from the reservoir during the period of the earthquake.

(e) The profiles of line marker movement for Series B models are shown in Figure 15, and indicate relatively little movement at the base of the slope and an increase in strain

above the base (at each depth this movement is the average value of three sets of markers, located 100 mm apart in a region mid-way up the slope). There is continuity between the lower saturated layers and the dry surface layer, and the dry surface layer itself is subject to large strains. It is noted here that mid-depth planes parallel to the base slope extend to the sand surface above the horizontal base of the toe, and deformation of surface and mid-depth layers is therefore free from end effects associated with shearing resistance beneath the toe.

(f) Figure 16 shows the movement of line markers at different depths within the slope plotted for each test against earthquake magnitude (the mean of positive and negative maximum peaks). The magnitude of deformation recorded beneath the Series B slopes (18° slope, 40 % relative density) indicates a strong dependence on earthquake magnitude. This suggests that inertial effects predominate in the mechanism of deformation associated with the 18" slopes. Within the slope there is negative pore pressure generation (Figure 10) and deformation is not therefore associated with a loss of shearing resistance.

(g) Figure 16 suggests a limiting earthquake magnitude of between 18 and 20 % of g, below which no displacement will take place at any depth.

(h) The depth of flow recorded by pore pressure transducers in Test NP12, Figure 8, is typical for Series B tests. The position of these transducers is shown in Figure 3. Although the phreatic surface in the region of the toe appears to be in a transient state (somewhat exaggerated in Figure 8 by the scaling factors used), flow from the front edge of the toe is very much greater than flow into the region of the rising phreatic surface (Pilgrim, 1994): flowlines are already parallel to the phreatic surface (as in the

steady state) and do not intersect the phreatic surface (as in a truly transient state) (Cedergren, 1967).

Results: Series C

(a) In all the Series C models a stainless steel plate was fitted over the horizontal base at the toe of the slope, and the models were built with a drain to control seepage from the toe. In Tests NP15 and NP16 a wedge of sand failed (graben formation) at the toe of the slope during the earthquake. There is no evidence of graben formation in Test NP17 but in these three tests a pressure ridge formed at the front edge of the toe. In Test NP18 seepage had not reached the toe of the slope at the time the earthquake was fired and there is no evidence of either graben formation or a pressure ridge.

(b) As with the Series B tests, video film shows that in Series C tests NP15, NP16 and NP17 movement of the slope surface takes place predominantly during the earthquake and not before.

(c) Base and surface acceleration records are shown for Test NP15 in Figure 14. There is a loss of transmission (magnitude), while the phase lag of the surface layer increases during shaking to over 150" . The analogy with a second order linear system suggests that the natural frequency of the sand mass has been reduced by softening (the positive pore pressures shown in Figure 11) to below the fundamental driving frequency. This degree of softening beneath the gentle slopes is also illustrated by the double amplitude pore pressures recorded in Test NP17 (Figure 12), which indicate a condition of cyclic mobility following initial liquefaction.

(d) The profiles of line marker movement for Series C Tests can be seen in Figure 17, and indicate relatively little movement at the base of the slope and an increase in strain

above the base. There is continuity between the lower saturated layers and the dry surface layer. The dry surface layer itself is relatively free of strain in **Tests** NP 16 and NP17. The surface layer in the Series C slopes is dry and is not subject to transient pore pressure increase and loss of shearing resistance. It is apparent that inertial effects on these gentle slopes do not cause large dynamic shear stresses and deformation is therefore relatively small. Test NP18 differed from the other tests in that seepage had not fully developed at the time the earthquake was fired (Pilgrim, 1994). However this resulted in an interesting difference as shown in the magnitude of observed deformation (although a small error is apparent in the measurement of surface movement).

(e) Figure 18 shows the movement of line markers at different depths within the slope plotted for each test against earthquake magnitude. The magnitude of deformation recorded beneath the Series C slopes (6" slope, 40 % relative density) shows no dependence on earthquake magnitude. This suggests that deformation of the 6" slopes is driven by static stresses (gravity effects) following transient pore pressure increase and loss of shearing resistance. The earthquake is instrumental in generating these large positive pore pressures but inertial effects do not play a significant part in the mechanism of deformation.

(f) It is apparent that for earthquakes of magnitude less than 25 % of g the more gentle 6" slopes suffer greater deformation than the steeper 18" slopes.

(g) The depth of flow recorded by Test NP16, Figure 9, is typical for Series C tests. The location of these transducers is the same as that shown in Figure 5 (but with PPT 3962 at Z = +100 mm). Steady state seepage has been established before the earthquake is fired.

CONCLUSION

The results from an experimental programme carried out on the Cambridge Geotechnical Centrifuge have been presented. The main objective was to establish empirical data with which to clarify the nature of continuous deformation beneath sand slopes of gentle to moderate inclination. Discrete slip planes have not been observed, the predominant form of instability is through shear strain deformation. Two loading conditions are associated with the observed mechanisms of slope deformation:

(a) Inertial loading, which is the direct impact of the earthquake and is predominant in mechanisms associated with deformation of slopes of moderate inclination.
(b) Transient pore pressure increase, which causes the loss of shearing resistance due to partial liquefaction (and subsequent gravity effects) and is predominant in mechanisms associated with deformation of gentle slopes.

The interpretation of moment by moment deformation requires more rigorous theoretical investigation, and is considered in a companion paper (Pilgrim, 1995).

ACKNOWLEDGEMENTS

The paper was written while the author was resident in Tokyo at the invitation of Professors Kenji Ishihara and Ikuo Towhata, and supported by a grant of the Kajima Foundation. The author would also like to express his gratitude to the family of Professor and Mrs. Masamichi Tsuboi for their kindness and hospitality during his stay in Tokyo.

REFERENCES

Arulmoli, K., Muraleetharan, K.K., Hossain, M.M. & Fruth, L.S. (1992). VELACS laboratory testing programme soil data report. The Earth Technology Corporation, 13900 Alton Parkway, Suite 120, Irvine, CA 92718, U.S.A.

Bolton, M.D. (1986). The strength and dilatancy of sands. Geotechnique 36, No. 1, 65-78.

Cedergren, H.R. (1967). Seepage, drainage and flownets (2nd. edition 1977), pp. 115-118, 127-139, 159-163. John Wiley & Sons.

O'Rourke, T.D., Roth, B.L & Hamada, M. (1989). A case study of large ground deformation during the 1971 San Fernando Earthquake. Proc. 2nd. U.S.-Japan Workshop on Liquefaction, Large Ground Deformation and their Effects on Lifelines, Buffalo, pp. 50-66.

Pilgrim, N.K. (1994). Observation and analysis of slope stability with seepage in centrifuge model earthquakes. Ph.D. Thesis. Cambridge University, U.K., pp. 24-39.

Pilgrim, N.K. (1995). Earthquake related deformation beneath gently inclined ground. Submitted to Soils and Foundations, January 1995.

Sasaki, Y., Towhata, I., Tokida, K., Yamada, K., Matsumoto, H., Tamari, Y. & Saya, S. (1992). Mechanism of permanent displacement of ground caused by seismic liquefaction. Soils and Foundations 32, No. 3, 79-96.

Schofield, A.N. (1980). Cambridge geotechnical centrifuge operations. The Twentieth Rankine Lecture. Geotechnique 30, No. 3, 227-268.

Schofield, A.N. (198 1). Dynamic and earthquake geotechnical centrifuge modelling. Proc. Int. Conf. Recent Advances in Geotechnical Earthquake Engineering and Soil Dynamics, St. Louis, pp. 1081-l 100.

Steedman, R.S. (1989). Centrifuge modelling of large ground motions and their effects on structures. Proc. 2nd. U.S.-Japan Workshop on Liquefaction, Large Ground Deformation and their Effects on Lifelines, Buffalo, pp. 218-232.

Towhata, I., Sasaki, Y., Tokida, K., Matsumoto, H., Tamari, Y. & Yamada, K. (1992). Prediction of permanent displacement of liquefied ground by means of minimum energy principle. Soils and Foundations 32, No. 3, 97-l 16.

Yasuda, S., Hamada, M., Wakamatsu, K. & Morimoto, I. (1989). Liquefaction induced permanent ground displacements in Niigata city. Proc. 2nd. U.S.-Japan Workshop on Liquefaction, Large Ground Deformation and their Effects on Lifelines, Buffalo, pp. 67-8 1.

Parameter	I Value
G (specific gravity)	**2.67**
e_{max}	**0.887**
e_{min}	0.551
ϕ_{crit}	**33”**
Constant head permeability at 40.2 % relative density	**0.066** mm/sec

Table 1: Properties of Nevada sand (after Arulmoli et al, 1992)

Test	Slope (°) and depth (mm)	Slope at toe (°)	Toe plate and toe drain	Constant reservoir depth (mm)	Eq. mag. (% of g)	Graben observed
NP11	18/80	21	Yes/No	40	26.1	Yes
NP12	18/80	22	No/Yes	33	20.1	No
NP13	18/80	18	Yes/No	33	22.1	Yes
NP14	18/80	19	No/Yes	39	30.8	No
NP15	6/100	17	Yes/Yes	76	32.6	Yes
NP16	6/100	18	Yes/Yes	77	25.1	Yes
NP17	6/100	18	Yes/Yes	82	20.1	No
NP18	6/100	17	Yes/Yes	transient	28.2	No

Earthquake magnitude is the mean of positive and negative maximum peaks.

Table 2: Summary of test data

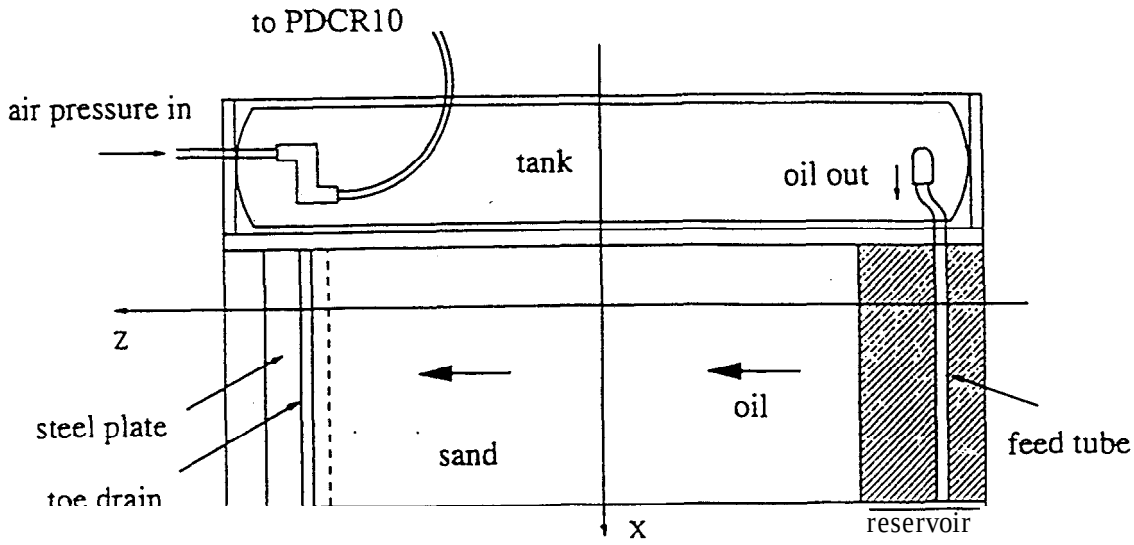

Figure 1: The experimental package

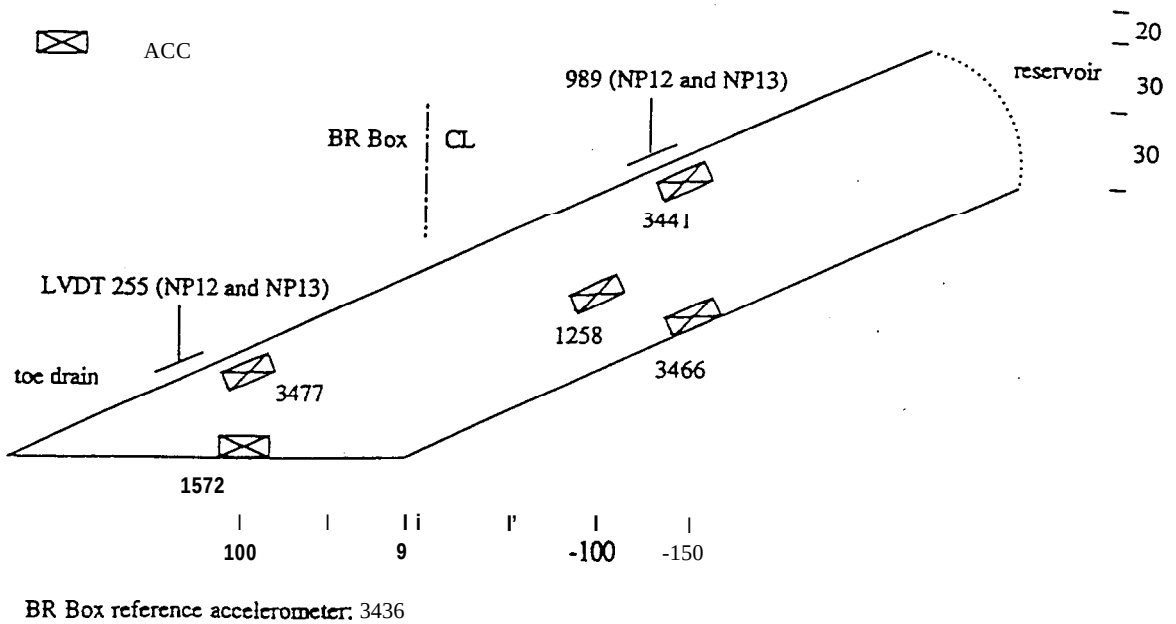

Figure 2: Series B models, accelerometers

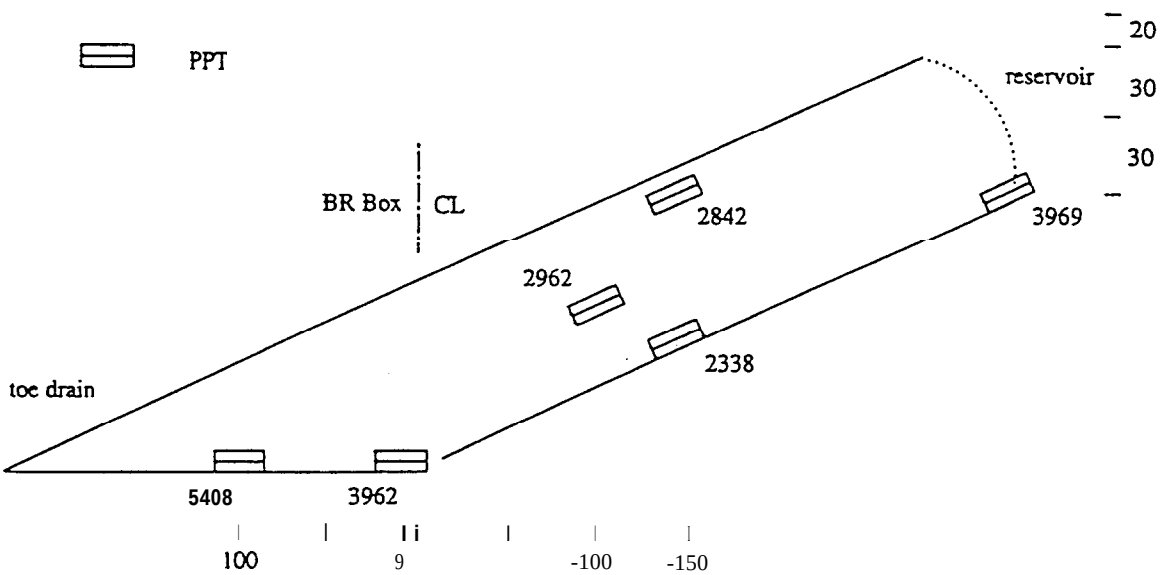

Figure 3: Series B models, pore pressure transducers

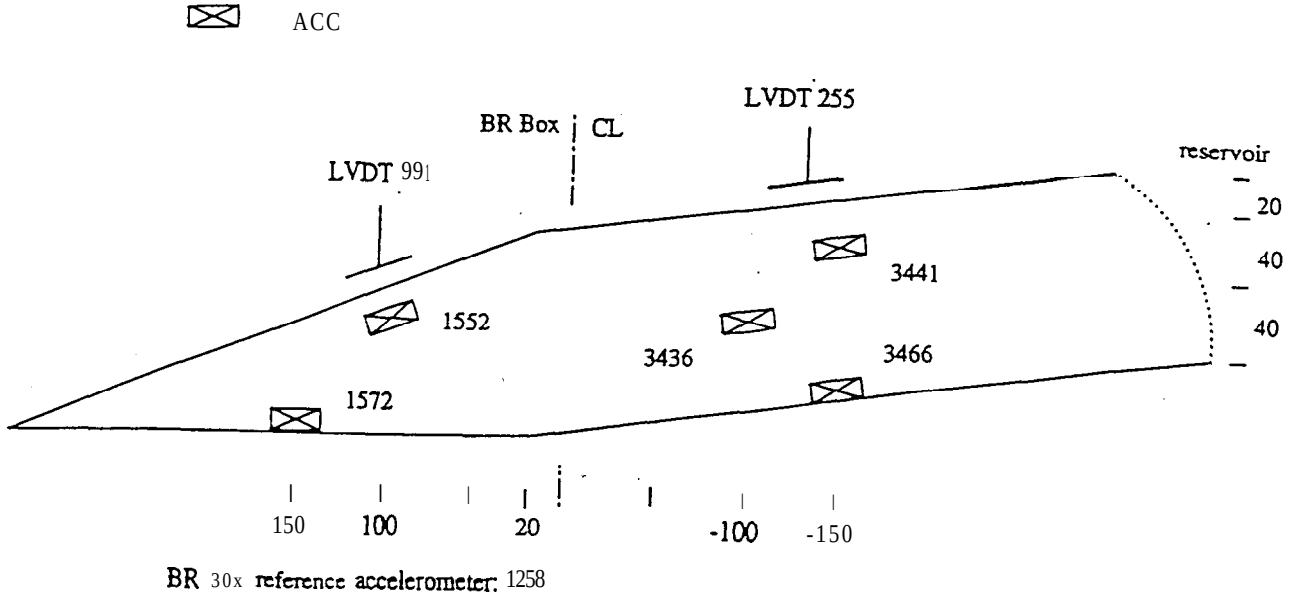

Figure 4: Test NP 15, accelerometers

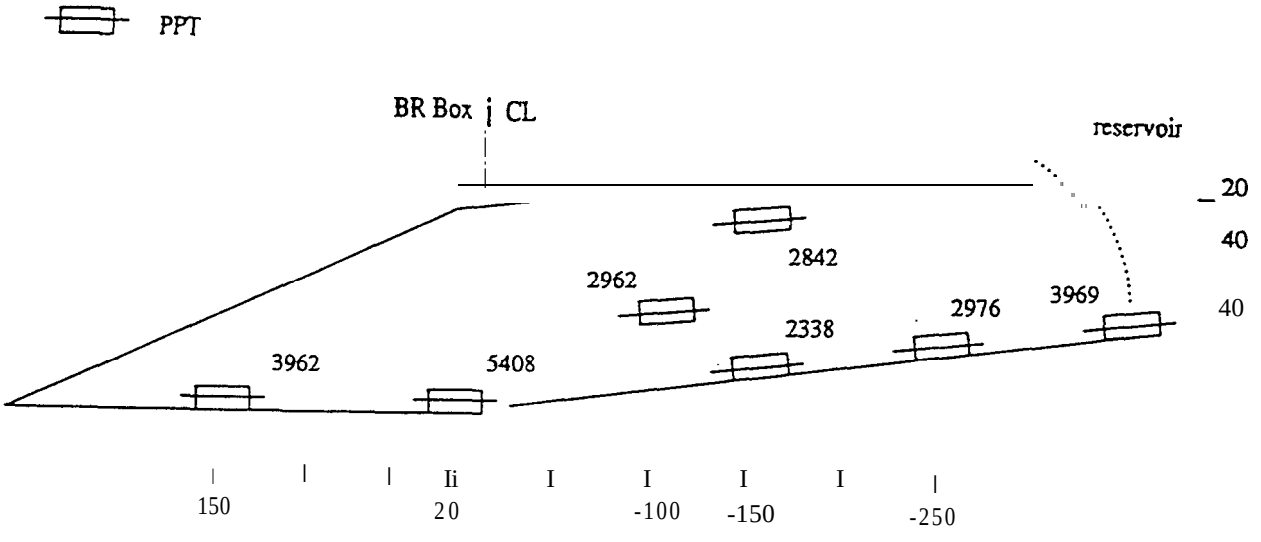

Figure 5: Test NP 15, pore pressure transducers

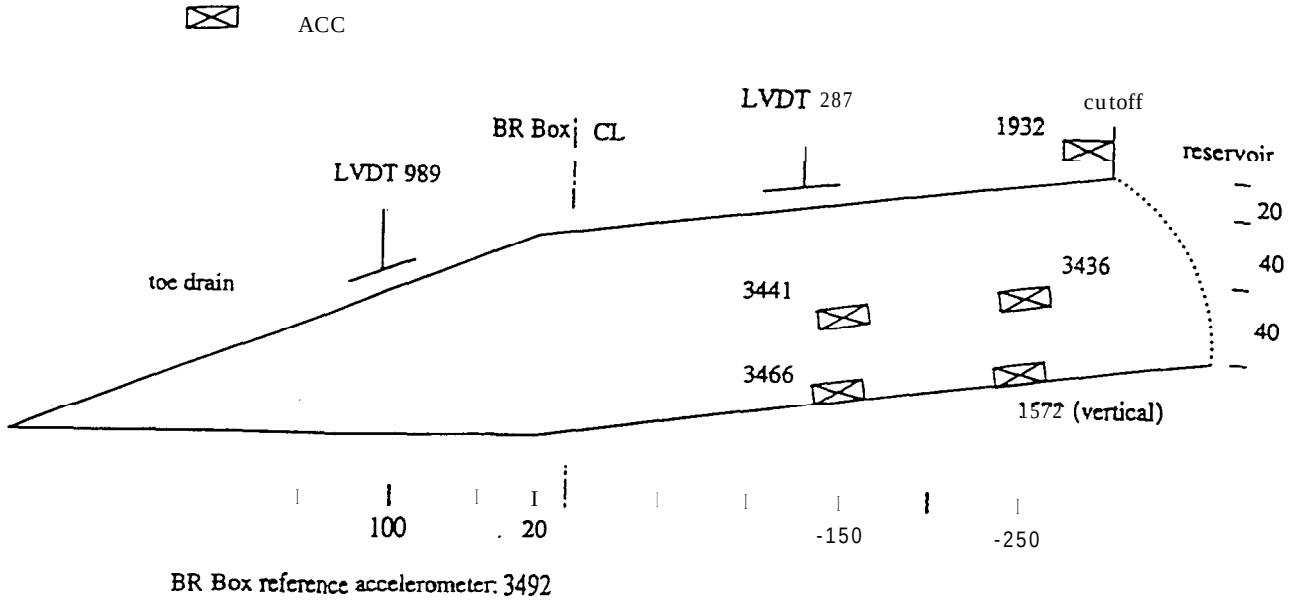

Figure 6: Test NP 17, accelerometers

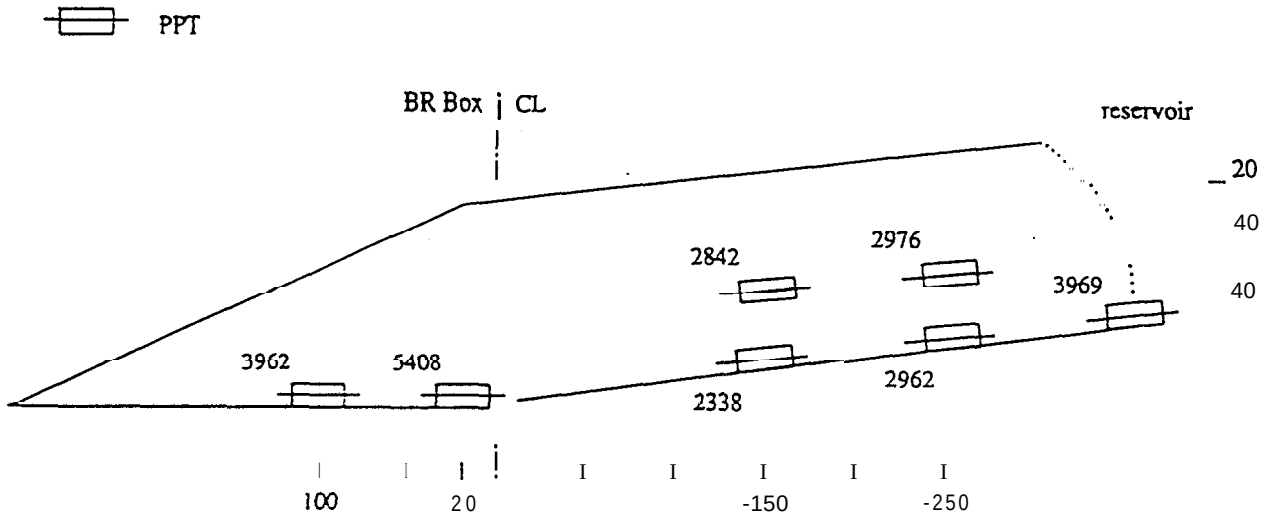

Fig&e 7: Test NP 17, pore pressure transducers

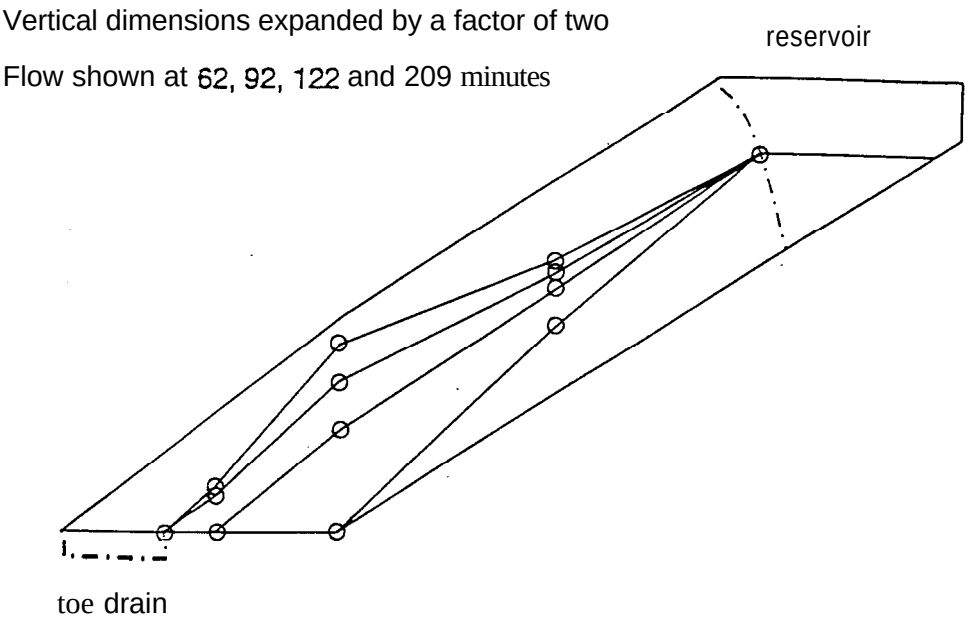

Figure 8: Test NP 12, development of seepage

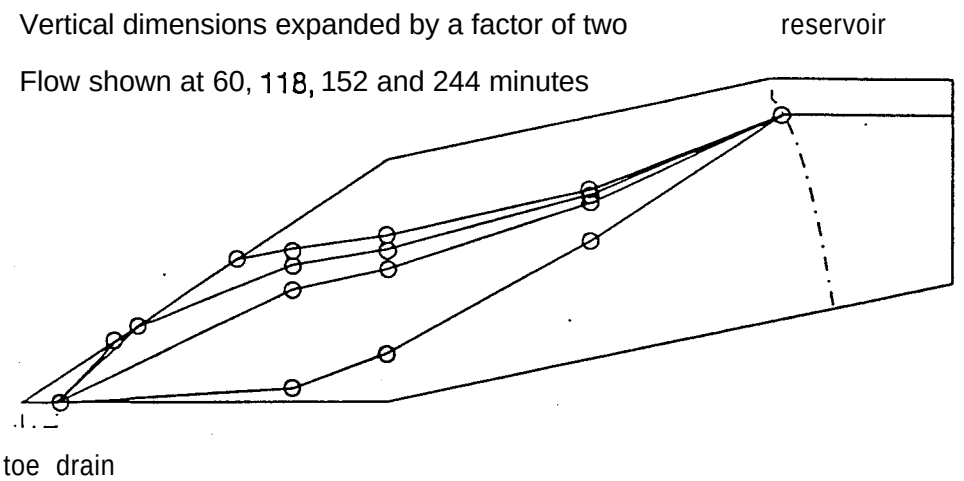

Figure 9: Test NP 16, development of seepage

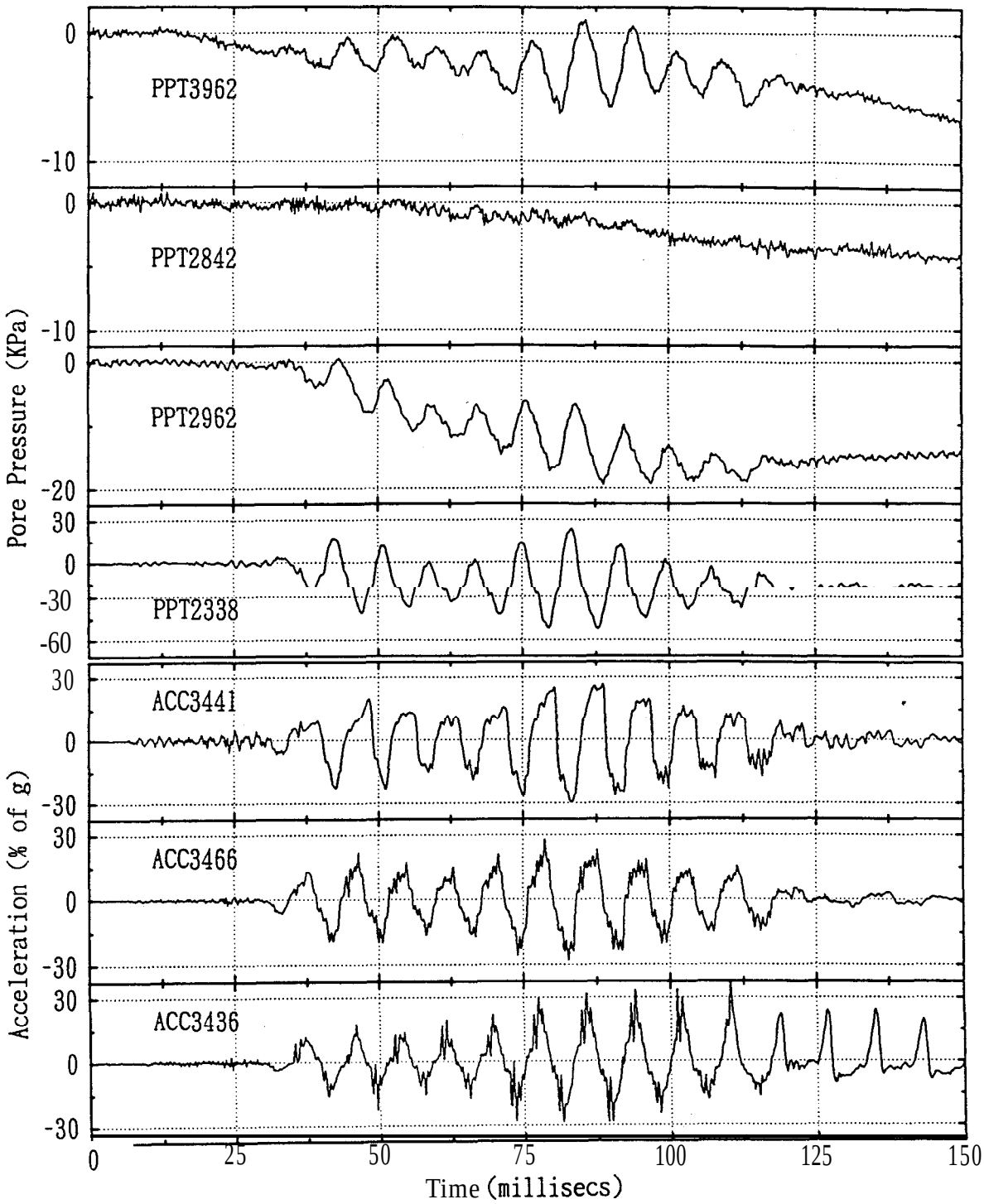

Figure 10: Test NP14, time records

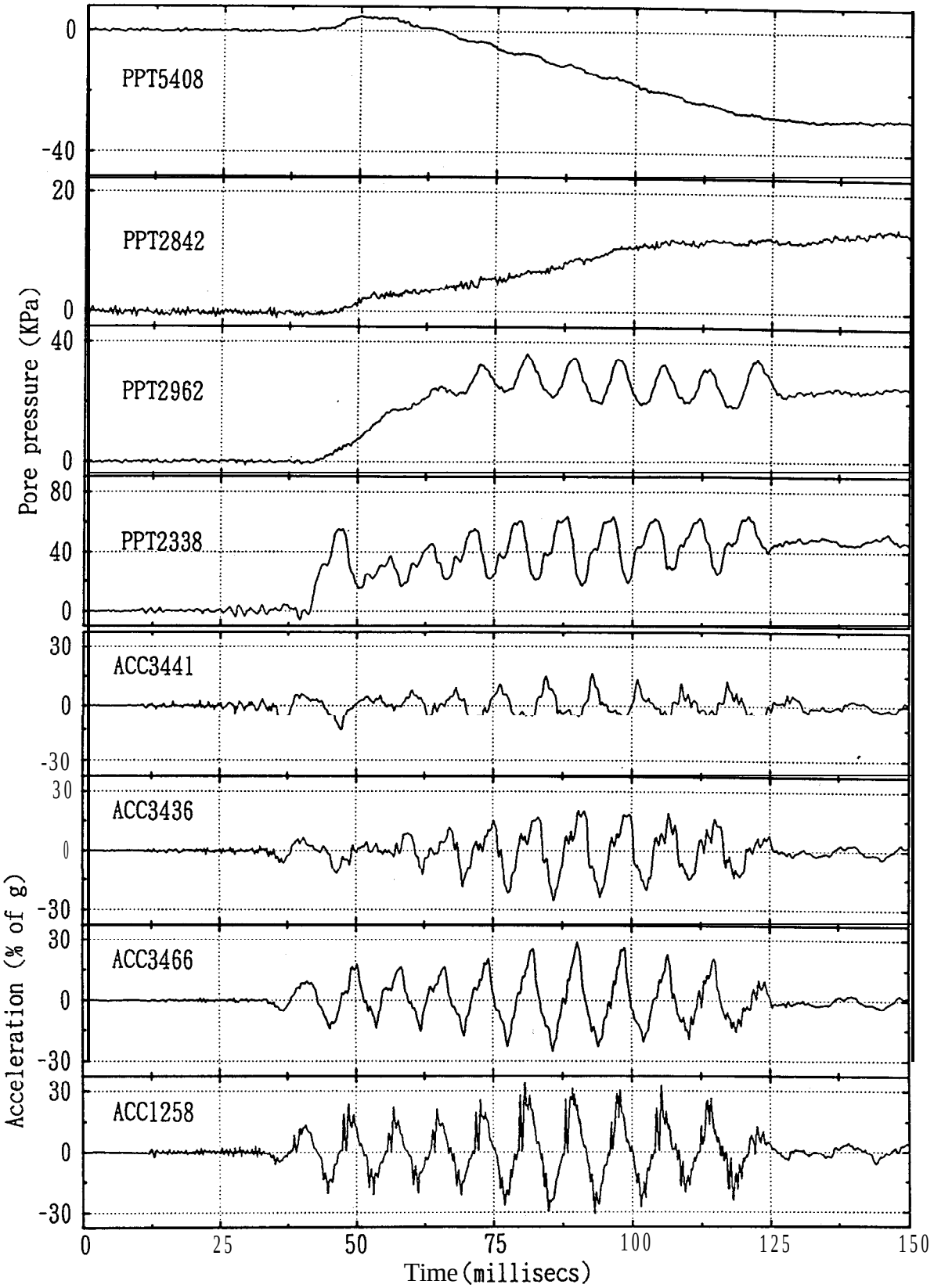

Figure 11: Test NP15, time records

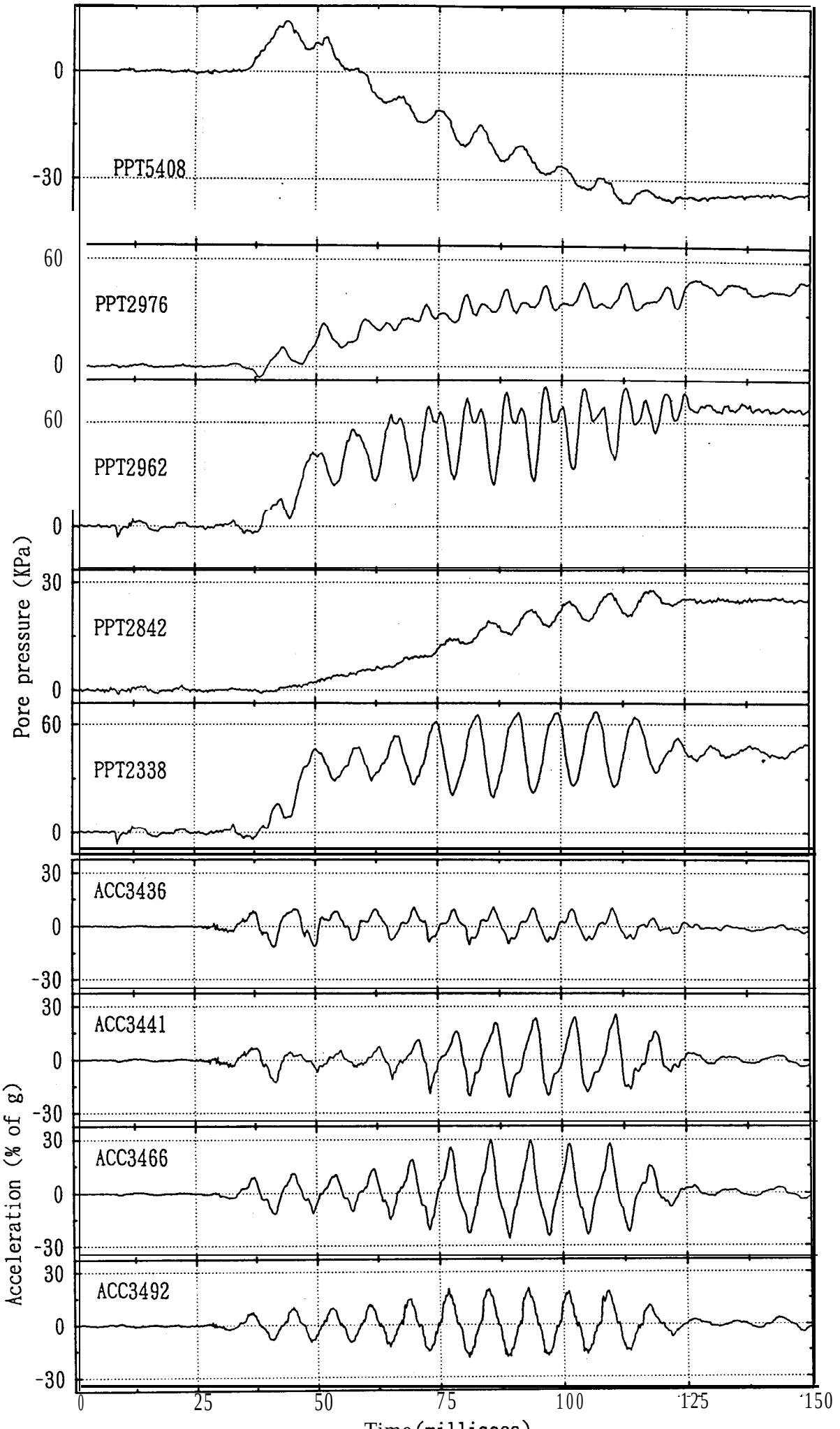

Figure 12: Test NP17, time records

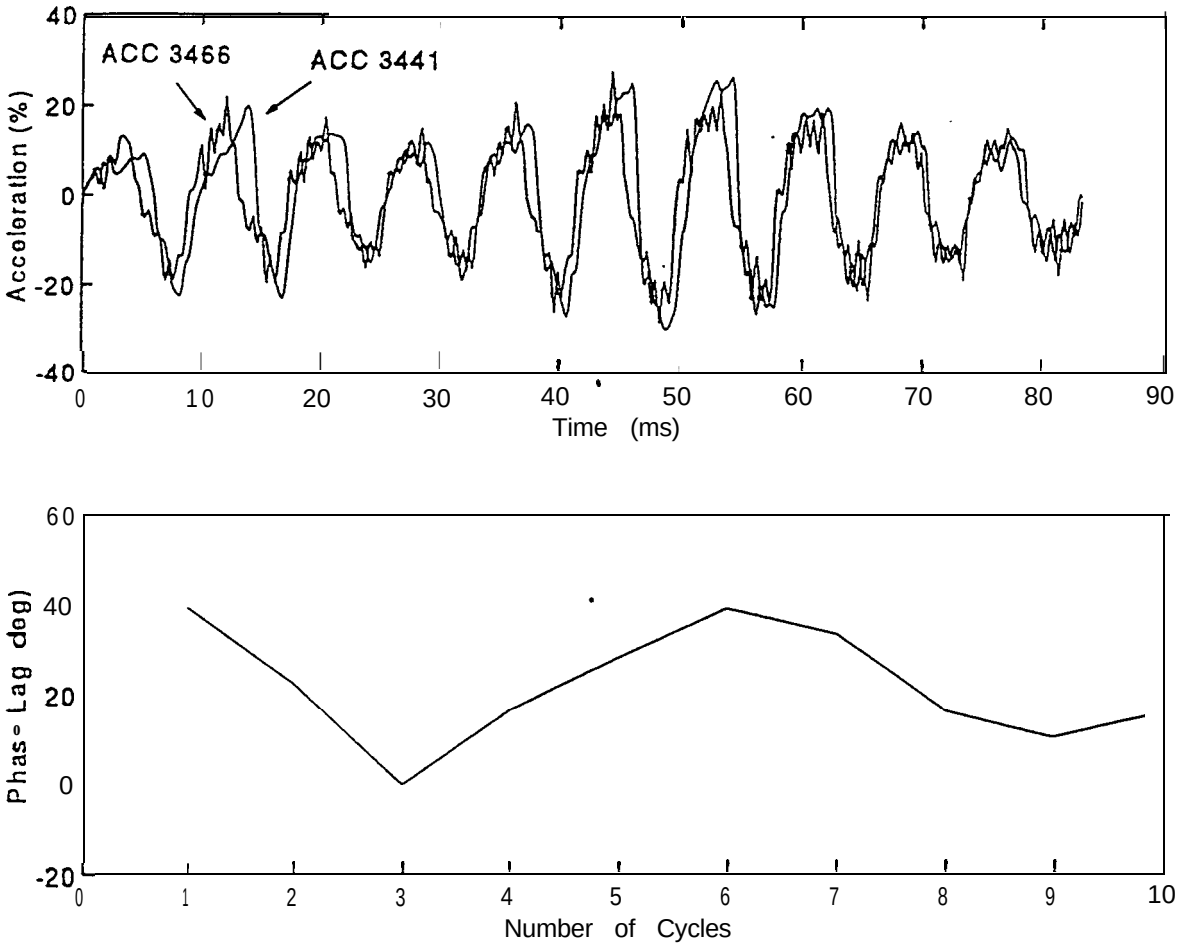

Figure 13: Test NP14, acceleration and phase difference

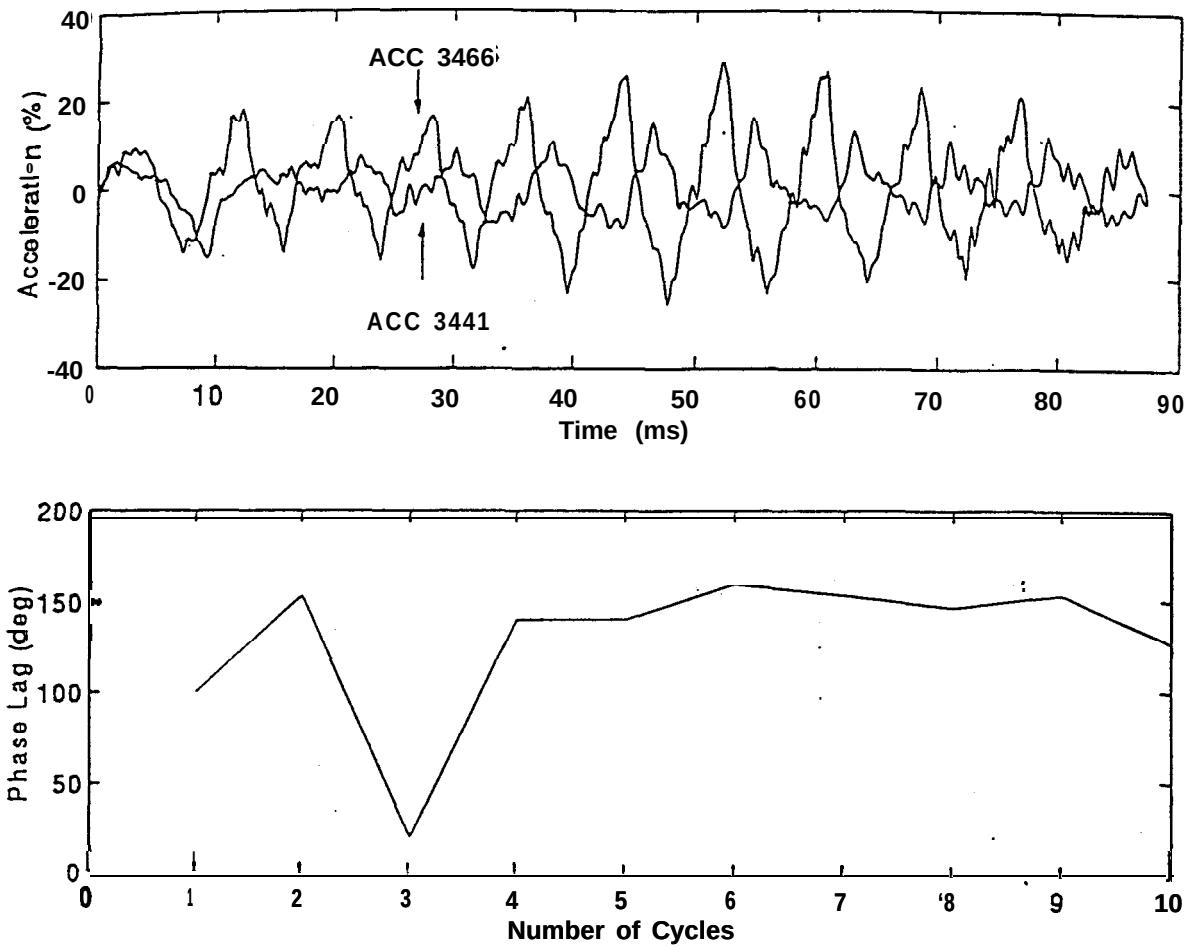

Figure 14: Test NP15, acceleration and phase difference

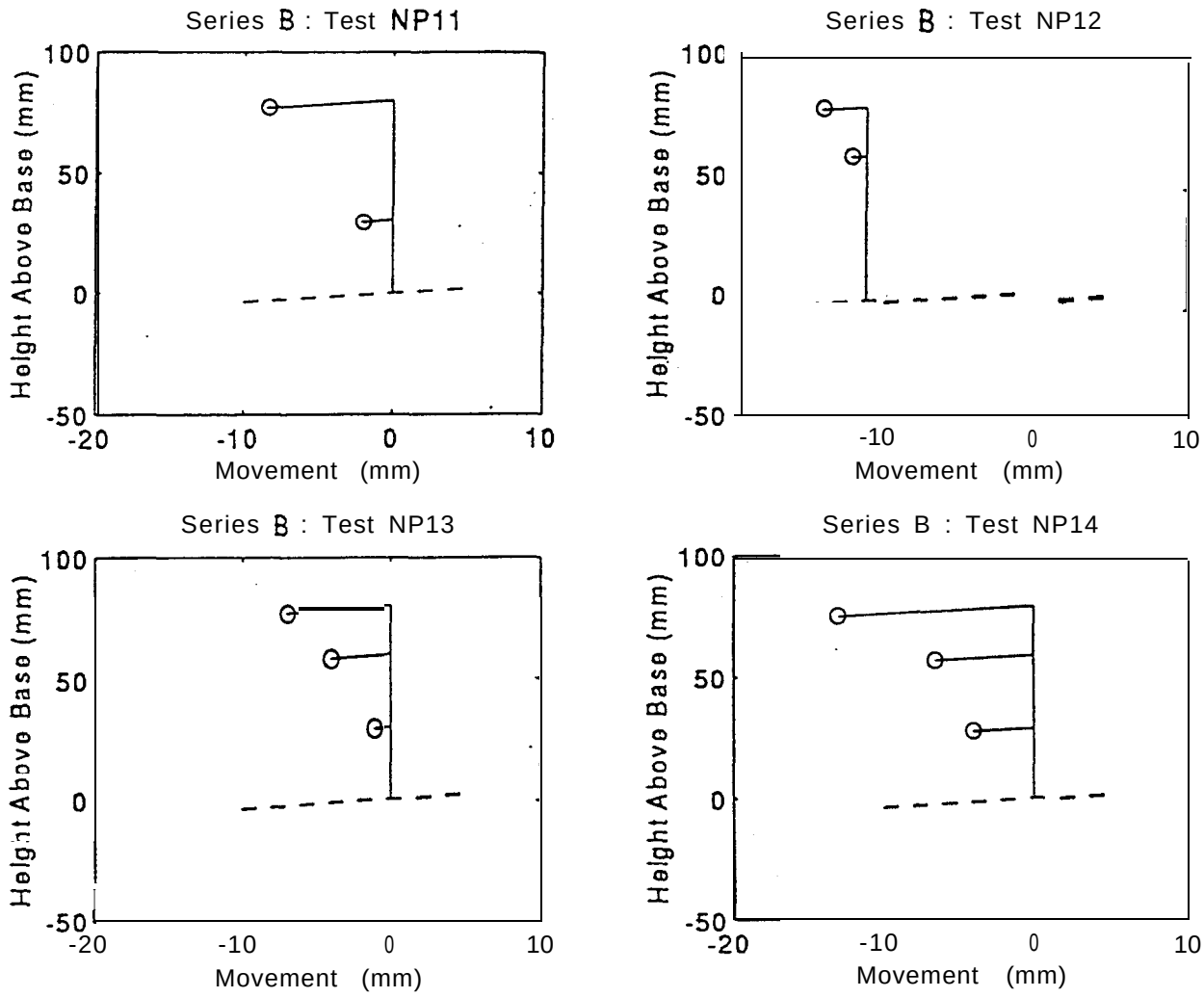

Figure 15: Series B, profiles of deformation

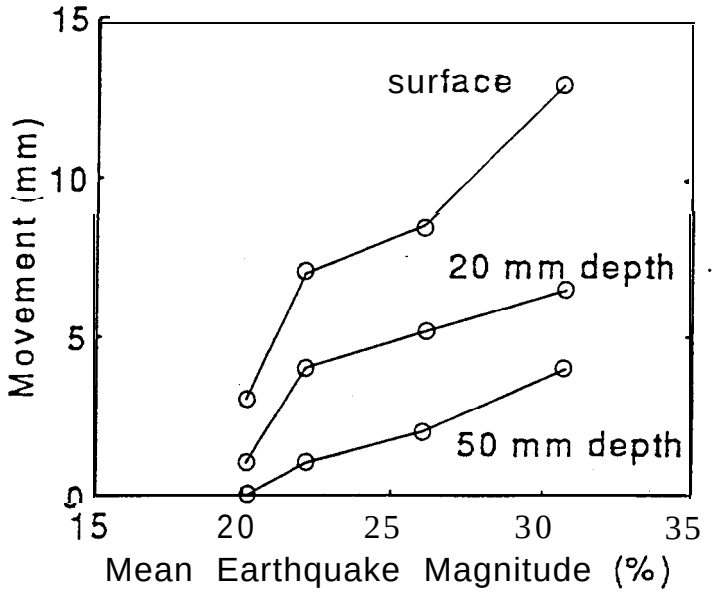

Figure 16: Series B, deformation and earthquake magnitude

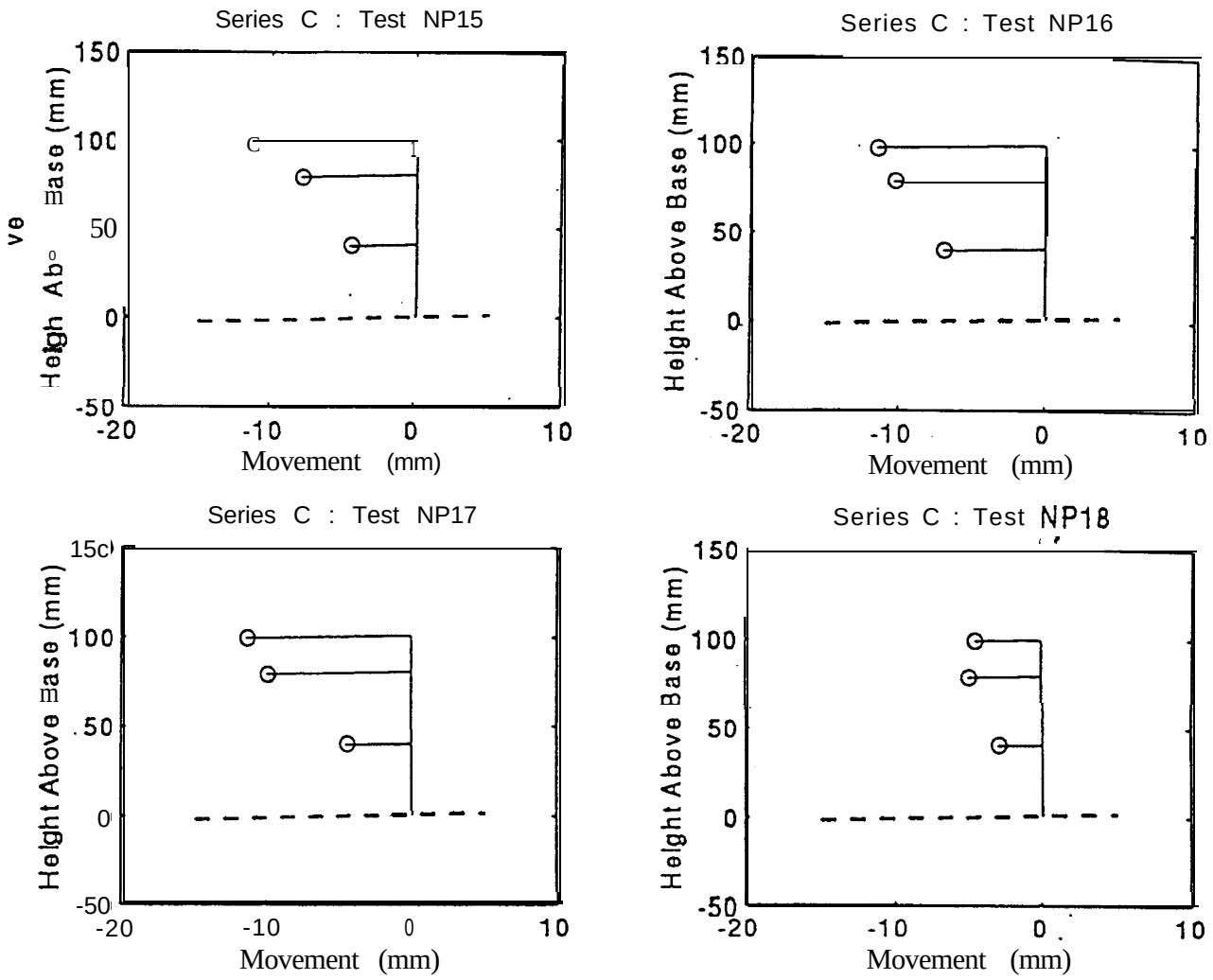

Figure 17: Series C, profiles of deformation

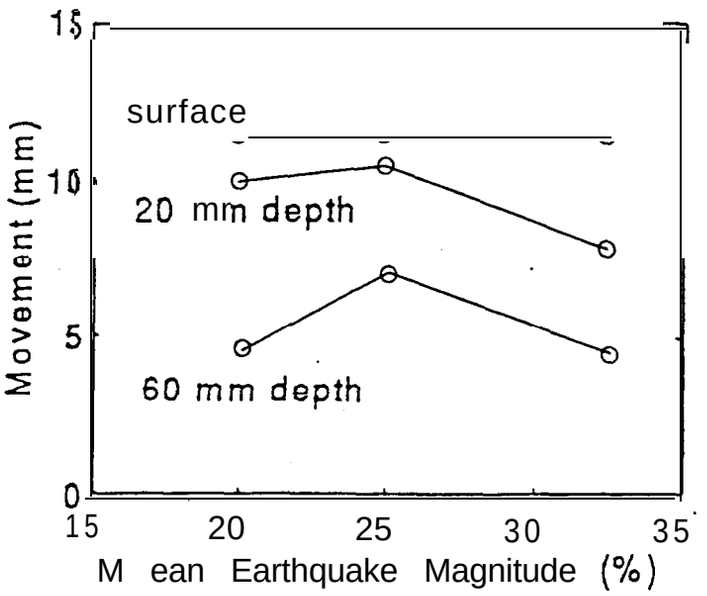

Figure 18: Series C, deformation and earthquake magnitude